Correlated Rydberg Electromagnetically Induced Transparencys

Lei Huang, Peng-fei Wang, Han-xiao Zhang, Yu Zhu, Hong Yang, and Dong Yan

School of Physics and Electronic Engineering, Hainan Normal University, Haikou 571158, P. R. China

In the regime of Rydberg electromagnetically induced transparency, we study the correlated behaviors between the transmission spectra of a pair of probe fields passing through respective parallel one-dimensional cold Rydberg ensembles. Due to the van der Waals (vdW) interactions between Rydberg atoms, each ensemble exhibits a local optical nonlinearity, where the output EIT spectra are sensitive to both the input probe intensity and the photonic statistics. More interestingly, a nonlocal optical nonlinearity emerges between two spatially separated ensembles, as the probe transmissivity and probe correlation at the exit of one Rydberg ensemble can be manipulated by the probe field at the input of the other Rydberg ensemble. Realizing correlated Rydberg EITs holds great potential for applications in quantum control, quantum network, quantum walk and so on.

In the `twocolumn` layout and without the `titlepage` option a paragraph without a previous section title may directly follow the abstract. In `onecolumn` format or with a dedicated `titlepage`, this should be avoided.

1

Rydberg atoms, which are neutral atoms in a state of high principal quantum number, are often called big atoms with exaggerated physical properties [1]. These unusual properties result from the large orbit radius of Rydberg atoms, including long radiative lifetimes, high polarizability and large electric dipole moments. Due to their high polarizability and large electric

dipole moments, Rydberg atoms strongly interact with other Rydberg atoms [2, 3] and are extremely sensitive to the surrounding electric fields [4]. Undoubtedly, these features make them the natural candidates for studying many-body physics [5, 6, 7, 8] and for precise measurement [9, 10, 11, 12, 13, 14, 15].

In addition, the effect of electromagnetically induced transparency (EIT) [16], as is well known in the field of quantum optics, could allow for an effective quantum interface between atoms and light without absorption. In general, photons do not directly interact with each other. However, by employing the EIT technique, the strong interactions between Rydberg atoms can be mapped onto photons, causing photons to become either strongly attractive or repulsive [17, 18]. Based on the modification of photonic statistics, the combination of EIT with Rydberg atoms allows us to investigate nonlinear quantum optics at the single-photon level [19] and explore quantum information applications, such as building single photon sources [20], quantum gate [21], transistors [22, 23], filters [24], subtractors [25, 26], and switches [27, 28].

Unlike typical linear EIT realized in an ensemble of independent atoms, Rydberg EIT spectra of the transmitted probe intensity can be influenced by the dipole blockade effect, where the excitation of two or more atoms into a Rydberg state within a mesoscopic volume is forbidden due to the dipole-dipole interaction. Specifically, the transmission coefficient and the photonic correlations become highly sensitive to the input probe intensity. Theoretical and experimental investigations on Rydberg EIT have recently attracted intense interest [29, 30, 31, 32, 33, 34, 35, 36, 37, 38, 39, 40, 41, 42, 43, 44, 45, 46, 47, 48, 49, 50]. To date, most investigations on Rydberg EIT have focused on one-dimensional systems, while studies on two-dimensional systems—specifically, to

Dong Yan: latex@quantum-journal.org, http://quantum-journal.org

the best of our knowledge, studies on correlated Rydberg EITs—remain quite rare.

In this paper, we investigate the correlated optical responses of two probe fields passing through closely spaced, parallel one-dimensional samples of cold Rydberg atoms in the EIT regime. Each EIT spectrum exhibits cooperative optical nonlinearities when the input probe intensity is strong enough. Moreover, by varying the input probe intensity of one probe field and keeping other parameters unchanged, we observe alterations in both the transmitted probe intensity and the second-order correlation function of the other probe field. Additionally, we thoroughly examine the extent to which one probe field is influenced by changing the other probe field. The realization of correlated Rydberg EITs enables quantum manipulation, the construction of quantum networks, the testing of quantum walk, and more.
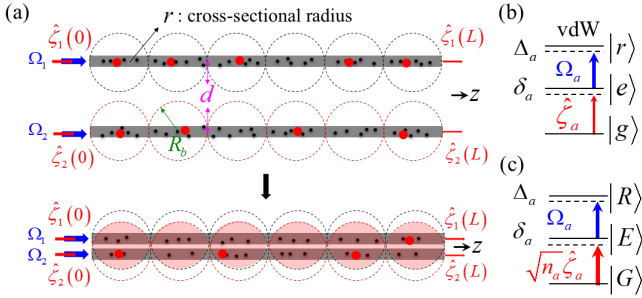

Figure 1: (Color online) (a) Upper: Two weak laser fields, $\hat{\zeta}_1$ and $\hat{\zeta}_2$, propagate through two independent, parallel, one-dimensional atomic ensembles in the presence of the classical control fields Ω_1 and Ω_2. In this case, $d \gg R_b \gg r$. Lower: The optical responses of the two weak laser fields are correlated by the vdW interactions when $R_b \gg d \sim r$. Throughout this paper, we use the values $R_b = 14.68~\mu$m, $d = 0.5~\mu$m, and $r = 0.5~\mu$m for the numerical calculations. A rugby-shaped shaded region forms a shared blockade area, created by the overlap of two blockade spheres. (b) Atomic levels. A weak probe field (Rabi frequency operator $\hat{\zeta}_a$ and detuning δ_a) and a classical coupling field (Rabi frequency Ω_a and detuning Δ_a) couple the ground state $|g\rangle$, intermediate state $|e\rangle$ and Rydberg state $|r\rangle$, respectively. vdW represents the long-range van der Waals interaction. (c) A superatom is composed of three collective states $|G\rangle$, $|E\rangle$ and $|D\rangle$. In comparison to the single-atom case, the collective coupling strength between states $|G\rangle$ and $|E\rangle$ is increased by a factor of $\sqrt{n_a}$ (a=1,2).

2 Model and Equations

As shown in Fig.1, we consider two parallel one-dimensional ^{87}Rb ultracold atomic samples, separated by the distance d, both having the same cross-sectional radius r and length L. In a-th ($a = 1, 2$) atomic sample, a weak laser field $\hat{\zeta}_a = g\hat{\mathcal{E}}_a$ with g the single atom coupling constant [51] and detuning δ_a propagates in the atomic sample in the presence of a classical control field Ω_a with detuning Δ_a. The level scheme of the ensemble atoms is shown in Fig.1(b), $|g\rangle$, $|e\rangle$ and $|r\rangle$ are the ground state, the excited state, and the highly excited Rydberg state of ^{87}Rb atoms, respectively. Specifically, these states refer to $|g\rangle = |5S_{1/2}, F = 1\rangle$, $|e\rangle = |5P_{3/2}\rangle$ and $|r\rangle = |90S\rangle$. The classical control field drives the upper transition $|e\rangle \rightarrow |r\rangle$, while the weak laser field couples the lower transition $|g\rangle \rightarrow |e\rangle$. Together, they drive the Rydberg atom into the three-level ladder-type configuration.

When an atom in the a-th atomic sample located at z_{ia} and an atom in the b-th atomic sample located at z_{jb} are excited to the Rydberg states, they experience strong long-range van der Waals (vdW) interactions, where $V_{ia,jb} = C_6/R_{ia,jb}^6$, with C_6 being the vdW coefficient and $R_{ia,jb} = |z_{ia} - z_{jb}|$ representing the distance between atoms. For $a = b$, the condition $i \neq j$ holds when considering interactions between different atoms within the same sample.

The Hamiltonian of the total system reads ($\hbar \equiv 1$)

$$\hat{H} = \sum_{a=1}^{2} \left(\hat{H}_a + \hat{V}_{aa} \right) + \hat{V}_{ab}, \qquad (1)$$

where $\hat{H}_a = \sum_j^N [\delta_a \hat{\sigma}_{ja}^{ee} + (\delta_a + \Delta_a) \hat{\sigma}_{ja}^{rr}] + [\hat{\zeta}_a \hat{\sigma}_{ja}^{eg} + \Omega_a \hat{\sigma}_{ja}^{er} + \text{H.c}]$ is the atom-light coupling in a-th atomic sample ($a = 1, 2$). $\hat{V}_{ab} = \sum_{i>j} V_{ia,jb} \hat{\sigma}_{ia}^{rr} \hat{\sigma}_{jb}^{rr}$ represents the vdW interaction between two atoms within the a-th atomic sample (when $a = b$) and the vdW interaction between two atoms in the a and b atomic samples (when $a \neq b$). Obviously, $\hat{V}_{ab}$ vanishes, while $\hat{V}_{aa}$ still exists in the limit of $d \rightarrow \infty$ (see upper schematic diagram in Fig.1(a)).

The dynamics of our system is governed by the following master equation

$$\dot{\varrho} = -i[\hat{H}, \varrho] + \mathcal{L}[\varrho], \qquad (2)$$

where ϱ and $\mathcal{L}[\varrho]$ are the density operator of the many-body system and Lindblad term,

2

which accounts for the incoherent processes, respectively. To solve the many-body equation (2), we can resort to the mean-field approximation. In the mean-field description, the many-body operators are replaced by their mean values and, consequently, the interparticle correlations are completely neglected. After defining the average atomic operator $\hat{\sigma}_a^{mn}(z) = \sum_{j=1}^{n} \hat{\sigma}_{ja}^{mn}(z)/n$ in the microvolume δV centered at z, the Heisenberg-Langevin equations for light and atomic operators in a-th atomic sample read [31]

$$
\begin{aligned}
\partial_t \hat{\mathcal{E}}_a(z) &= -c\partial_z \hat{\mathcal{E}}_a(z) + i\eta N \hat{\sigma}_a^{ge}(z), \\
\partial_t \hat{\sigma}_a^{ge}(z) &= -(i\delta_a + \gamma)\hat{\sigma}_a^{ge}(z) - ig\hat{\mathcal{E}}_a^\dagger(z) - i\Omega_a \hat{\sigma}_a^{gr}(z), \\
\partial_t \hat{\sigma}_a^{gr}(z) &= -i\left[\delta_a + \Delta_a + \hat{S}_{aa}(z) + \hat{S}_{ab}(z)\right]\hat{\sigma}_a^{gr}(z) \\
&\quad -\Gamma\hat{\sigma}_a^{gr}(z) - i\Omega_a \hat{\sigma}_a^{ge}(z),
\end{aligned}
\tag{3}
$$

where γ and Γ are the dephasing rate in state $|e\rangle$ and $|r\rangle$, respectively. $\hat{S}_{aa}(z) = \int d^3 z_a' \rho(z_a') C_6/|z_a - z_a'|^6 \hat{\sigma}_a^{rr}(z_a')$ and $\hat{S}_{ab}(z) = \int d^3 z_b' \rho(z_b') C_6/|z_a - z_b'|^6 \hat{\sigma}_b^{rr}(z_b')$ denote the interaction energy shift induced by inner Rydberg atoms in a-th atomic sample and the interaction energy shift induced by both a Rydberg atom in a-th atomic sample and all the Rydberg atoms in b-th atomic sample, respectively. Here, $\hat{S}_{aa}(z)$ and $\hat{S}_{ab}(z)$ have been translated into the frequency shift like $\delta_a + \Delta_a$. It means that the Rydberg transitions from $|g\rangle \to |r\rangle$ in a-th atomic sample are affected not only by the atoms within the sample but also the atoms in neighbor atomic sample. In general, both $\hat{S}_{aa}$ and $\hat{S}_{ab}$ are nonlocal in the sense that these quantities directly depend on the density of the atomic gas and Rydberg state population.

To reasonably estimate the effects induced by the frequency shifts $\hat{S}_{aa}(z)$ and $\hat{S}_{ab}(z)$, we use the superatom model, where all atoms share at most one Rydberg excitation in a blockade region. For simplicity, we first consider the case where $\hat{S}_{aa}(z) \neq 0$ while $\hat{S}_{ab}(z) = 0$. As shown the upper schematic in Fig.1(a), a Rydberg superatom (SA) can generally be regarded as a sphere with the blockade radius R_b due to the homogeneity and the isotropy. In the weak-probe limit, each independent SA has three collective states $|G_a\rangle = |g\rangle^{\otimes n_a}$, $|E_a\rangle = \sum_{j=1}^{n_a} |g_1, ..., e_j, ..., g_{n_a}\rangle/\sqrt{n_a}$ and $|R_a\rangle = \sum_{j=1}^{n_a} |g_1, ..., r_j, ..., g_{n_a}\rangle/\sqrt{n_a}$, where n_a is the number of atoms in the SA. These states form a three-level system as shown in Fig.1(c). Ac-

cordingly, we define the Rydberg SA excitation projection operator as $\hat{P}_a = |R_a\rangle\langle R_a|$.

Solving the Heisenberg-Langevin equations of independent SAs in the steady state, we can obtain the Rydberg excitation projection operator [31],

$$
\hat{P}_a(z) = \frac{n_a\eta^2 \hat{\mathcal{E}}_a^\dagger(z)\hat{\mathcal{E}}_a(z)\Omega_a^2}{n_a\eta^2 \hat{\mathcal{E}}_a^\dagger(z)\hat{\mathcal{E}}_a(z)\Omega_a^2 + [\Omega_a^2 - \delta_a(\delta_a + \Delta_a)\delta_a]^2 + \delta_a^2\gamma_a^2}
\tag{4}
$$

The polarizability of each probe field is conditioned upon its projection,

$$
\hat{\alpha}_a(z) = \hat{P}_a(z)\alpha_{\text{TLA}} + \left[\hat{1} - \hat{P}_a(z)\right]\alpha_{\text{TLL}}
\tag{5}
$$

with the polarizability of a two-level atom

$$
\alpha_{\text{TLA}} = \frac{i\gamma}{\gamma + i\delta_a}
\tag{6}
$$

and that of a three-level ladder atom

$$
\alpha_{\text{TLL}} = \frac{i\gamma}{\gamma + i\delta_a + \frac{\Omega_a^2}{\Gamma + i(\delta_a + \Delta_a)}}.
\tag{7}
$$

It is clear that the optical response of a SA depends on the Rydberg projection operator (4): it behaves like a two-level, absorptive medium when $\hat{\alpha}(z)$ reduces to α_{TLA} for $\hat{P}_a(z) = \hat{1}$. Alternatively, it behaves like a three-level, EIT medium when $\hat{\alpha}(z)$ reduces to α_{TLL} for $\hat{P}_a(z) = \hat{0}$.

The transmission of the each probe light is examined through the probe light intensity, defined as $I_a(z) = \langle\hat{\mathcal{E}}_a^\dagger(z)\hat{\mathcal{E}}_a(z)\rangle$. The atomic sample is no longer homogeneous, and in the steady state, the propagation equation of the intensity $I_a(z)$ follows

$$
\partial_z \langle\hat{\mathcal{E}}_a^\dagger(z)\hat{\mathcal{E}}_a(z)\rangle = -\kappa(z)\langle\text{Im}[\hat{\alpha}(z)]\hat{\mathcal{E}}_a^\dagger(z)\hat{\mathcal{E}}_a(z)\rangle,
\tag{8}
$$

where $\kappa(z) = \rho(z)\omega_p/(\epsilon_0 c\gamma)$ is the resonant absorption coefficient. The modification of the probe light intensity $I_a(z)$ is strongly dependent on the polarizability. If $\text{Im}[\hat{\alpha}(z)] = 0$, i.e., under the ideal EIT condition, the probe light intensity $I_a(z)$ remains unchanged in the EIT window. In general, it decays along the z-axis due to $\text{Im}[\hat{\alpha}(z)] > 0$.

Next, we remove $\text{Im}[\hat{\alpha}(z)]$ out of $\langle\text{Im}[\hat{\alpha}(z)]\hat{\mathcal{E}}_a^\dagger(z)\hat{\mathcal{E}}_a(z)\rangle$ in Eq. (8) and simultaneously replace $\hat{\mathcal{E}}_a^\dagger(z)\hat{\mathcal{E}}_a(z)$ with $\langle\hat{\mathcal{E}}_a^\dagger(z)\hat{\mathcal{E}}_a(z)\rangle g_a(z)$ in Eq.(4), by introducing the two-photon correlation function $g_a(z) =$

$\langle\hat{\mathcal{E}}_a^{\dagger 2}(z)\hat{\mathcal{E}}_a^2(z)\rangle/\langle\hat{\mathcal{E}}_a^\dagger(z)\hat{\mathcal{E}}_a(z)\rangle^2$ under the mean-field approximation.

Similarly, the propagation equation of two-photon correlation function $g_a(z)$ follows [31]

$$\partial_z g_a(z) = -\kappa(z)\hat{P}_a(z)\,\text{Im}[\alpha_{\text{TLA}} - \alpha_{\text{TLL}}]g_a(z) \tag{9}$$

Compared with probe light intensity $I_a(z)$, there's an additional possibility for two-photon correlation function $g_a(z)$: it can be amplified by the atomic medium when $\text{Im}[\alpha_{\text{TLA}}] < \text{Im}[\alpha_{\text{TLL}}]$.

When the two atomic samples are close but not coincident with $R_b \gg d \sim r$, both $\hat{S}_{aa}$ and $\hat{S}_{ab}$ are active in this regime. A single Rydberg excitation in the rugby-shaped shaded region (the mutual blockade region) can suppress further excitations not only within the atomic sample itself but also in the neighboring sample. Based on this, we employ a stochastic procedure to solve the coupled Eq. (4)-(9) with initial input probe light intensity $I_a(0)$ and its initial two-photon correlation function $g_a(0)$. We divide each sample into $N = L/(2R_b)$ and then simultaneously assess the Rydberg excitations of two SAs but in the same *rugby*. Specifically, $P_a(z)$ and $P_b(z)$ are calculated from Eq.(4) and compare them with the respective random number p_a and p_b, generated independently. There are three main cases: (I) If $P_a(z) < p_a$ and $P_b(z) < p_b$, set $P_a(z) = P_b(z) = 0$; (II) If $P_a(z) \geq p_a$ and $P_b(z) < p_b$, set $P_a(z) = 1$ and $P_b(z) = 0$ (or vice verse);(III) If $P_a(z) \geq p_a$ and $P_b(z) \geq p_b$, then if $P_a(z) > P_b(z)$, set $P_a(z) = 1$ and $P_b(z) = 0$ (or vice versa); otherwise, set $P_a(z) = P_b(z) = 0.5$. This evaluation is carried out one-by-one using Monte Carlo sampling. To obtain steady mean values, this procedure is typically repeated many times.

3 Results and discussion

The steady optical responses are examined using both the probe transmissivity $T_a = I_a(L)/I_a(0)$ and the probe correlation $G_a = g_a(L)/g_a(0)$ at the exist of each ensemble. In Fig.2, we present the probe transmissivities T_1 and T_2, and the probe correlations G_1 and G_2 by simultaneously varying their input probe light intensities $\zeta_1(0)=\zeta_2(0)$. It is clear that the optical responses of the two probe fields are identical and exhibit the typical nonlinearity: on one hand, the stronger the input probe field is, the greater
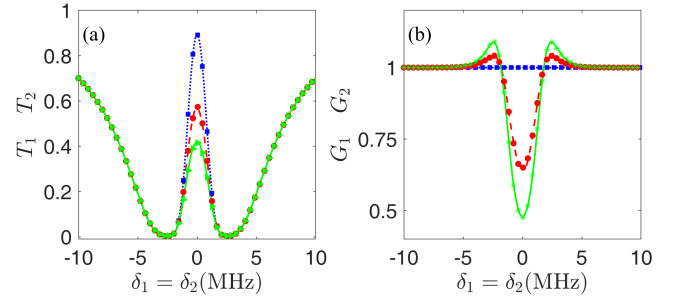

Figure 2: (Color online) (a) Probe transmissivities T_1 and T_2 and (b) the probe correlations G_1 and G_2 versus the probe detuning $\delta_1 = \delta_2$ for $(\zeta_1(0), \zeta_2(0)) = (0.1, 0.1)$ MHz (blue), $(0.7, 0.7)$ MHz (red), and $(1.0, 1.0)$ MHz (green) with initial two-photon correlation function $g_1(0) = g_2(0) = 1.0$. Lines with and without symbols represent the first and the second ensembles, respectively. Other parameters are $\Omega_1/2\pi = \Omega_2/2\pi = 2.5$ MHz, $\gamma_1/2\pi = \gamma_2/2\pi = 3.0$ MHz, $\Gamma_1/2\pi = \Gamma_2/2\pi = 10.0$ kHz, $C_6/2\pi = 140\,\text{GHz}\,\mu\text{m}^6$, $\rho = 1.5 \times 10^8\,\text{mm}^{-3}$, and $L = 1.0$ mm.

the absorption within the EIT window; on the other hand, the probe correlation is suppressed within the EIT window but is enhanced around the Aulter-Townes doublet $\Omega_{1(2)} \approx \pm 2.5$ MHz as the input probe intensity increases.

As a result, the initially classical input fields $(g_1(0) = g_2(0) = 1)$ are modified into anti-bunching fields $(g_1(L) = g_2(L) < 1)$ or bunching fields $(g_1(L) = g_2(L) > 1)$ between photons by the time they leave the respective ensemble.

Essentially, the symmetry in our system is also evident here. As shown in Fig. 3(a), T_1 and T_2 interchange as $\zeta_1(0)$ and $\zeta_2(0)$ are swapped, while all other parameters remain the same. Figure 3(b1) also displays this symmetry in the parameter space of the input probe light intensities $\zeta_1(0)$ and $\zeta_2(0)$. Figures 3(b2) and (b3) show that the probe transmissivity is no longer symmetric when the input probe light intensities are exchanged, provided the input two-photon correlation functions differ. For instance, even when $\zeta_1(0) = \zeta_2(0)$, the optical responses from two ensembles differ significantly (see the red circles in Figs. 3(b2) and (b3)). The condition $|T_1 - T_2| \neq 0$ indicates that fewer (or more) photons are absorbed in one ensemble while more (or fewer) photons are absorbed in the other, due to $g_1(0) \neq g_2(0)$. It is easy to deduce that the symmetry will be broken if different parameters are chosen for the two ensembles, such as the input probe light intensity or the input two-photon cor-
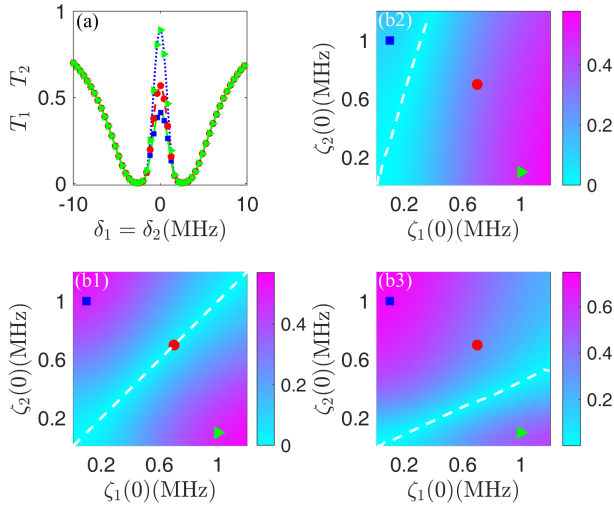
Figure 3: (color online). (a) Probe transmissivities T_1 and T_2 versus the probe detuning $\delta_1 = \delta_2$ for $(\zeta_1(0), \zeta_2(0)) = (0.1, 1.0)$ MHz (blue), $(0.7, 0.7)$ MHz (red), and $(1.0, 0.1)$ MHz (green). Lines with and without symbols correspond to the first and the second ensembles, respectively. (b1)-(b3) Diagrams of the absolute value $|T_2 - T_1|$ at $\delta_1 = \delta_2 = 0$ as a function of the input probe light intensities $\zeta_1(0)$ and $\zeta_2(0)$ for $g_1(0) = 1.0, 0.1$ and 5.0 with $g_2(0) = 1.0$. White dashed lines denote $|T_2 - T_1| = 0$. The blue square, red circle and green triangle mark $(\zeta_1(0), \zeta_2(0)) = (0.1, 1.0)$, $(0.7, 0.7)$ and $(1.0, 0.1)$, respectively. Other parameters are the same as in Fig.2.

relation function, as mentioned above, as well as the classical control field intensity, atomic density, and other parameters.
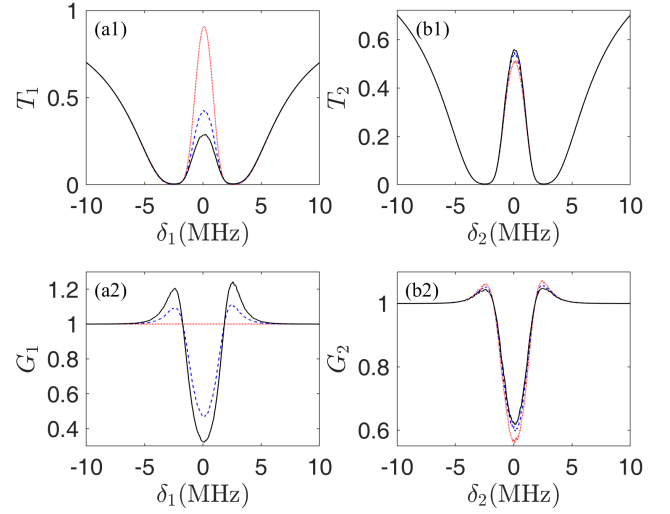

Figure 4: (color online). (a1)-(b1) Probe transmissivities T_1 and T_2, and (a2)-(b2) the probe correlations G_1 and G_2 versus their respective probe detunings δ_1 and δ_2 for $\zeta_1(0) = 0.1$ MHz (red dotted), 0.7 MHz (blue dashed), and 1.2 MHz (black solid) with $\zeta_2(0) = 1.0$ MHz. Other parameters are the same as in Fig.2.

We then examine the correlations between the optical responses at the two exits of the respective atomic ensembles. In Fig.4, we present the probe transmissivities T_1 and T_2 and the probe correlations G_1 and G_2 by varying $\zeta_1(0)$ while keeping $\zeta_2(0)$ fixed. As shown in Figs.4 (a1) and (a2), the first ensemble exhibits clearly optical nonlinearity as $\zeta_1(0)$ increases from 0.1 MHz to 1.2 MHz. Generally, the optical responses from the two atomic ensembles do not influence each other when the ensembles are completely separated (see the upper schematic diagram in Fig.1). However, As shown in Figs.4 (b1) and (b2) T_2 is enhanced by about 10% at $\delta_2 = 0$ without any parameters changes in the second ensemble. Correspondingly, G_2 is enhanced by about12% within the EIT window and is suppressed by 8% around the Aulter-Townes doublet $\Omega_{1(2)} \approx \pm 2.5$ MHz. This correlated phenomenon arises from the complex competition for excitation to the Rydberg state. Specifically, increasing the first input probe field may significantly enhance the probability of excitation to Rydberg state for atoms in the first ensemble and slightly reduce if for atoms in the second ensemble, as they share at most one Rydberg excitation within the same blockade region (a rugby-shaped area of the lower schematic dia-
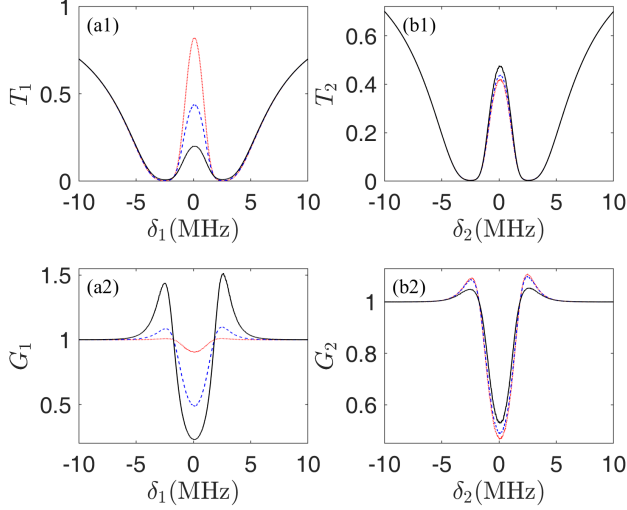
gram in Fig.1).

Figure 5: (color online). (a1)-(b1) Probe transmissivities T_1 and T_2, and (a2)-(b2) the probe correlations G_1 and G_2 versus their respective probe detunings δ_1 and δ_2 for $g_1(0) = 0.1$ (red-dotted), 1.0 (blue dashed), 5.0 (black solid) with $g_2 = 1.0$. Other parameters are the same as in Fig.2.

In addition, changing the input two-photon correlation function in one ensemble also affects the output optical responses of the other ensemble. Figure.5 shows at $\delta_2 = 0$ both T_2 and G_2 are enhanced by about 12%, while around the Aulter-Townes doublet G_2 is suppressed by approximately 12%. This occurs because a bigger two-photon correlation function in the first ensemble increases the probability that the ground-state atoms in the first ensemble will absorb photons. Consequently, the probability of excitation to Rydberg state for atoms in the second ensemble is reduced. Physically, this behavior results from nonlinear optical responses mediated by the Rydberg interaction.

Finally, to demonstrate the ability to manipulate the output optical response from one ensemble by adjusting the input optical parameters of the other, we plot the growth rate of the second probe transmissivities by varying the input probe light intensities in Fig. 6(a) and the input probe correlation function in Fig. 6(b). Figure 6(a) shows that η is nearly zero when $\zeta_1 \leq 0.4$ MHz or $\zeta_2 \leq 0.4$ MHz. In this regime, manipulation is not possible because the input probe light intensities are too weak to excite the Rydberg state in either ensembles, preventing an effective correlation between them. Beyond this threshold, manipulation becomes feasible as the Rydberg in-
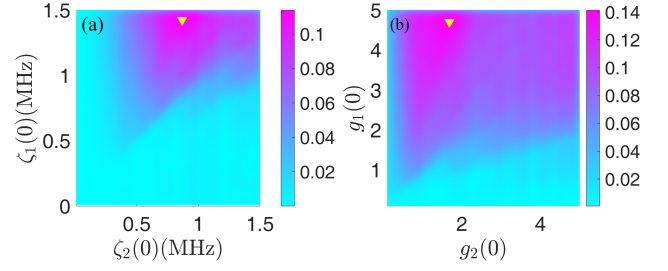

Figure 6: (color online). (a) Diagram of the growth rate of the second probe transmissivities $\eta(\zeta_1(0), \zeta_2(0)) = T_2(\zeta_1(0), \zeta_2(0))/T_2(\zeta_1(0), \zeta_2^0(0)) - 1$ with $\zeta_2^0(0) \equiv 0.01$ MHz as a function of the input probe light intensities $\zeta_1(0)$ and $\zeta_2(0)$ for $g_1(0) = g_2(0) = 1.0$. (b) Diagram of the growth rate of the second probe transmissivities $\eta(g_1(0), g_2(0)) = T_2(g_1(0), g_2(0))/T_2(g_1(0), g_2^0(0)) - 1$ with $g_2^0(0) \equiv 1.0$ as a function of the input two-photon correlation functions $g_1(0)$ and $g_2(0)$ for $\zeta_1(0) = \zeta_2(0) = 1.0$ MHz. The yellow triangle denotes the maximal growth rate. Other parameters are the same as in Fig.2.

teraction between the two ensembles takes effect. η always increases with increasing ζ_1, but initially increases and then decreases with decreasing ζ_2. The maximal growth rate of 14% is achieved at $(\zeta_2, \zeta_1) = (0.8, 1.0)$ MHz.

Figure 6(b) shows that the growth rate η is nearly zero when $g_1 \leq 0.6$ or $g_2 \leq 0.2$. In this case, although the input probe light intensity is strong enough, this light with $g_2 \ll 1$ provides too few photons to excite the Rydberg state within a given volume. Therefore, manipulation is ineffective because competition for excitation to Rydberg state between the two ensembles can not occur. Similar to the input probe light intensities, η consistently increases with increasing g_1, and initially increases with increasing g_2 until $g_2 = 0.8$, after which it decreases. The maximal growth rate of 14% occurs at $(g_2, g_1) = (0.8, 1.0)$. Overall, the most effective manipulation is achieved when the primary optical parameters exceed the secondary ones, i.e., $\zeta_2 > \zeta_1$ and $g_2 > g_1$.

4 Conclusions

In summary, we have investigated the correlated steady-state optical responses between two probe fields passing through closely spaced, parallel one-dimensional samples of cold Rydberg atoms. Under the condition of optical nonlinearity, the EIT spectrum of one ensemble can be modified by varying the input probe intensity and the two-

photon correlation function of the other ensemble. This capability enables us to perform quantum manipulation with Rydberg ensembles. Furthermore, we systematically investigate the effectiveness of this quantum manipulation. This model can be expanded to multiple Rydberg ensembles to build quantum network and explore quantum work.

Acknowledgements

References

[1] Gallagher T. F. Rydberg Atoms (Cambridge University Press, Cambridge, UK, **1994**).

[2] Gallagher T. F.; Pillet P. Dipole-dipole interactions of Rydberg atoms. *Adv. At. Mol. Opt. Phys.* **2008**, *56*, 161.

[3] Comparat D. P.; Pillet P. Dipole blockade in a cold Rydberg atomic sample. *J. Opt. Soc. Am. B* **2010**, *27*, 208.

[4] Saffman M.; Walker T. G.; Mølmer K. Quantum information with Rydberg atoms. *Rev. Mod. Phys.* **2010**, *82*, 2313.

[5] Labuhn H.; Barredo D.; Ravets S.; Léséleuc S.; Macri T.; Lahaye T.; Browaeys A. Tunable two-dimensional arrays of single Rydberg atoms for realizing quantum Ising models. *Nature* **2016**, *534*, 667.

[6] Bernien H.; Schwartz S.; Keesling A.; Levine H.; Omran A.; Pichler H.; Choi S.; Zibrov A. S.; Endres M.; Greiner M.; Vuletić V.; Lukin M. D. Tunable two-dimensional arrays of single Rydberg atoms for realizing quantum Ising models. *Nature* **2017**, *551*, 579.

[7] Guardado-Sanchez E.; Brown P. T.; Mitra D.; Devakul T.; Huse D. A.; Schauß P.; Bakr W. S. Probing the Quench Dynamics of Antiferromagnetic Correlations in a 2D Quantum Ising Spin System. *Phys. Rev. X* **2018**, *8*, 021069.

[8] Browaeys A.; Lahaye T. Many-body physics with individually controlled Rydberg atoms. *Nat. Phys.* **2020**, *16*, 132.

[9] Sedlacek J. A.; Schwettmann A.; Kübler H.; Löw R.; Pfau T.; Shaffer J. P. Microwave electrometry with Ryd- berg atoms in a vapour cell using bright atomic resonances. *Nat. Phys.* **2012**, *8*, 819.

[10] Anderson D. A.; Schwarzkopf A.; Miller S. A.; Thaicharoen N.; Raithel G.; Gordon J. A.; Holloway C. L. Two-photon microwave transitions and strong-field effects in a room-temperature Rydberg-atom gas. *Phys. Rev. A* **2014**, *90*, 043419.

[11] Facon A.; Dietsche E. K.; Grosso D.; Haroche S.; Raimond J. M.; Brune M.; Gleyzes S. A sensitive electrom- eter based on a Rydberg atom in a Schrödinger-cat state. *Nature* **2016**, *535*, 262.

[12] Cox K. C.; Meyer D. H.; Fatemi F. K.; Kunz P. D. Quantum-limited atomic receiver in the electrically small regime. *Phys. Rev. Lett.* **2018**, *121*, 110502.

[13] Liao K.-Y.; Tu H.-T.; Yang S.-Z.; Chen C.-J.; Liu X.-H.; Liang J.; Zhang X.-D.; Yan H.; Zhu S.-L. Microwave electrometry via electromagnetically induced absorption in cold Rydberg atoms. *Phys. Rev. A* **2020**, *101*, 053432.

[14] Ding D.-S.; Liu Z.-K.; Shi B.-S.; Guo G.-C.; Mølmer K; Adams C. S. Enhanced metrology at the critical point of a many-body Rydberg atomic system. *Nat. Phys.* **2022**, *18*, 1447.

[15] Cui Y.; Jia F.-D.; Hao J.-H.; Wang Y.-H.; Zhou F.; Liu X.-B.; Yu Y.-H.; Mei J.; Bai J.-H.; Bao Y.-Y.; Hu D.; Wang Y.; Liu Y.; Zhang J.; Xie F.; Zhong Z.-P. Extending bandwidth sensitivity of Rydberg-atom-based microwave electrometry using an auxiliary microwave field. *Phys. Rev. A* **2023**, *107*, 043102.

[16] S. E. Harris. Electromagnetically Induced Transparency. *Phys. Today* **1997**, *36*, 36-42.

[17] Gorshkov A. V.; Nath R.; Pohl T. Dissipative Many-Body Quantum Optics in Rydberg Media. *Phys. Rev. Lett.* **2013**, *110*, 153601.

[18] Liang Q.-Y; Venkatramani A. V.; Cantu S. H.; Nicholson T. L.; Gullans M. J.; Gorshkov A. V.; Thompson J. D.; Chin C.; Lukin M. D.; Vuletic V. Observation of three-photon bound states in a quantum nonlinear medium. *Science* **2018**, *359*, 783.

[19] Firstenberg O.; Adams C. S.; Hofferber S. Nonlinear quantum optics mediated by Rydberg interactions. *J. Phys. B: At. Mol. Opt. Phys.* **2016**, *49*, 152003.

[20] Walker T. G. Strongly interacting photons. *Nature* **2012**, *488*, 39.

[21] Müller, M.; Lesanovsky, I.; Weimer, H.; Buchler, H. P.; Zoller, P. Mesoscopic Rydberg Gate Based on Electromagnetically Induced Transparency. *Phys. Rev. Lett.* **2009**, *102*, 170502.

[22] Gorniaczyk H.; Tresp C.; Schmidt J.; Fedder H.; Hofferberth S. Single-Photon Transistor Mediated by Interstate Rydberg Interactions. *Phys. Rev. Lett.* **2014**, *113*, 053601.

[23] Tiarks D.; Baur S.; Schneider K.; Dürr S.; Rempe G. Single-Photon Transistor Using a Förster Resonance. *Phys. Rev. Lett.* **2014**, *113*, 053602.

[24] Peyronel T.; Firstenberg O.; Liang Q.-Y.; Hofferberth S.; Gorshkov A. V.; Pohl T.; Lukin M. D.; Vuletic V. Quantum nonlinear optics with single photons enabled by strongly interacting atoms. *Nature*, **2012**, *488*, 57.

[25] Honer J.; Löw R.; Weimer H.; Pfau T.; Büchler H. P. Artificial Atoms Can Do More Than Atoms: Deterministic Single Photon Subtraction from Arbitrary Light Fields. *Phys. Rev. Lett.* **2011**, *107*, 093601.

[26] Gorshkov A. V.; Otterbach J.; Fleischhauer M.; Pohl T.; Lukin M. D.; Photon-Photon Interactions via Rydberg Blockade. *Phys. Rev. Lett.* **2011**, *107*, 133602.

[27] Chen W.; Beck K. M.; Bücker R.; Gullans M.; Lukin M. D.; Tanji-Suzuki H.; Vuletić V. All-Optical Switch and Transistor Gated by One Stored Photon. *Science* **2013**, *341*, 768.

[28] Baur S.; Tiarks D.; Rempe G.; Dürr S. Single-Photon Switch Based on Rydberg Blockade. *Phys. Rev. Lett.* **2014**, *112*, 073901.

[29] Weatherill K. J.; Pritchard J. D.; Abel R. P.; Bason M. G.; Mohapatra A. K.; Adams C. S. Electromagnetically induced transparency of an interacting cold Rydberg ensemble. *J. Phys. B: At. Mol. Opt. Phys.* **2008**, *41*, 201002.

[30] Pritchard J. D.; Maxwell D.; Gauguet A.; Weatherill K. J.; Jones M. P. A.; Adams C. S. Cooperative Atom-Light Interaction in a Blockaded Rydberg Ensemble. *Phys. Rev. Lett.* **2010**, *105*, 193603.

[31] Petrosyan D.; Otterbach J.; Fleischhauer M.; Electromagnetically Induced Transparency with Rydberg Atoms. *Phys. Rev. Lett.* **2011**, *107*, 213601.

[32] Pritchard J. D.; Gauguet A.; Weatherill K. J.; Adams C. S. Optical non-linearity in a dynamical Rydberg gas. *J. Phys. B: At. Mol. Opt. Phys.* **2011**, *44*, 184019.

[33] Reslen J. Many-body effects in a model of electromagnetically induced transparency. *J. Phys. B: At. Mol. Opt. Phys.* **2011**, *44*, 195505.

[34] Ates C.; Sevinçli S.; Pohl T. Electromagnetically induced transparency in strongly interacting Rydberg gases. *Phys. Rev. A* **2011**, *83*, 041802.

[35] Yan D.; Liu Y.-M.; Bao Q.-Q.; Fu C.-B.; Wu J.-H. Electromagnetically induced transparency in an inverted-Y system of interacting cold atoms. *Phys. Rev. A* **2012**, *86*, 023828.

[36] Yan D.; Cui C.-L.; Liu Y.-M.; Song L.-J.; Wu J.-H. Normal and abnormal nonlinear electromagnetically induced transparency due to dipole blockade of Rydberg excitation. *Phys. Rev. A* **2013**, *87*, 023827.

[37] Firstenberg O.; Peyronel T.; Liang Q.-Y.; Gorshkov A. V.; Lukin M. D.; Vuletić V. Attractive photons in a quantum nonlinear medium. *Nature* **2013**, *502*, 71.

[38] Jen H. H.; Wang D.-W. Theory of electromagnetically induced transparency in strongly correlated quantum gases. *Phys. Rev. A* **2013**, *87*, 061802.

[39] Gärttner M.; Evers J. Nonlinear absorption and density-dependent dephasing in Rydberg electromagnetically-induced-transparency media. *Phys. Rev. A* **2013**, *88*, 033417.

[40] Stanojevic J.; Parigi V.; Bimbard E.; Ourjoumtsev A.; Grangier P. Dispersive optical nonlinearities in a Rydberg electromagnetically-induced-transparency medium. *Phys. Rev. A* **2013**, *88*, 053845.

[41] Li W.; Viscor D.; Hofferberth S.; Lesanovsky I. Electromagnetically Induced Transparency in an Entangled Medium. *Phys. Rev. Lett.* **2014**, *112*, 243601.

[42] Liu Y.-M.; Yan D.; Tian X.-D.; Cui C.-L.; Wu J.-H. Electromagnetically induced transparency with cold Rydberg atoms: Superatom model beyond the weak-probe approximation. *Phys. Rev. A* **2014**, *89*, 033839.

[43] Liu Y.-M.; Tian X.-D.; Yan D.; Zhang Y.; Cui C.-L.; Wu J.-H. Nonlinear modifications of photon correlations via controlled single and double Rydberg blockade. *Phys. Rev. A* **2015**, *91*, 043802.

[44] Tresp C.; Bienias P.; Weber S.; Gorniaczyk H.; Mirgorodskiy I.; Büchler H. P.; Hofferberth S. Dipolar Dephasing of Rydberg D-State Polaritons C. *Phys. Rev. Lett.* **2015**, *115*, 083602.

[45] Liu Y.-M.; Wang X.; Tian X.-D.; Yan D.; Wu J.-H. Cooperative nonlinear grating sensitive to light intensity and photon correlation. *Opt. Lett.* **2016**, *41*, 408.

[46] Yan D.; Wang B.-B.; Bai Z.-Y.; Li W.-B. Electromagnetically induced transparency of interacting Rydberg atoms with two-body dephasing. *Opt. Express* **2020**, *28*, 9677.

[47] Tebben A.; Hainaut C.; Salzinger A.; Geier S.; Franz T.; Pohl T.; Gärttner M.; Zürn G.; Weidemüller M. Nonlinear absorption in interacting Rydberg electromagnetically-induced-transparency spectra on two-photon resonance. *Phys. Rev. A* **2021**, *103*, 063710.

[48] Su H.-J.; Liou J.-Y.; Lin I-C; Chen Y.-H. Optimizing the Rydberg EIT spectrum in a thermal vapor. *Opt. Express* **2022**, *30*, 1499.

[49] Srakaew K.; Weckesser P.; Hollerith S.; Wei D.; Adler D.; Bloch I.; Zeiher J. A subwavelength atomic array switched by a single Rydberg atom. *Nat. Phys.* **2023**, *19*, 714.

[50] Ou Y.; Huang G.-X. Switch and phase shift of photon polarization qubits via double Rydberg electromagnetically induced transparency. *Phys. Rev. A* **2024**, *109*, 023508.

[51] Scully M. O.; Zubairy M. S. Quantum Optics (Cambridge University Press, Cambridge, England, **1997**).